Journal of Membrane Science 640 (2021) 119858

Contents lists available at ScienceDirect

Journal of Membrane Science

journal homepage: www.elsevier.com/locate/memsci

Phenolic membranes with tunable sub-10-nm pores for nanofiltration and tight-ultrafiltration

Qianqian Lan [a], Chao Feng [a], Kaiqin Ou [a], Zicheng Wang [a], Yong Wang [b,*], Tianxi Liu [a,**]

[a] The Key Laboratory of Synthetic and Biological Colloids, Ministry of Education, School of Chemical and Material Engineering, Jiangnan University, Wuxi 214122, Jiangsu, PR China

[b] State Key Laboratory of Materials-Oriented Chemical Engineering, College of Chemical Engineering, Nanjing Tech University, Nanjing 211816, Jiangsu, PR China

ARTICLE INFO

Keywords:
Nanoporous phenolic
Separation membrane
Sub-10 nm
Nanofiltration
Tight-ultrafiltration

ABSTRACT

Membranes with sub-10-nm pores are receiving growing interest in recognizing and separating nanocolloids, biomolecules, and soluble salts from water, but suffer from difficulty of optimizing pore structures and inferior stability. Herein, we report an efficient method for the preparation of robust nanoporous phenolic membranes with widely tunable pore sizes in the range of nanofiltration and tight-ultrafiltration. Solutions of resol precursors and poly(ethylene glycol)s (PEGs) are spin-coated to form thin films and then heated to thermopolymerize resols into phenolics. Subsequently, the films are treated in H_2SO_4 solution to degrade PEGs, producing nanoporous phenolic membranes. Thus-prepared phenolic membranes exhibit adjustable effective pore sizes and tunable separation performances from nanofiltration to tight-ultrafiltration, which is otherwise inaccessible. Due to the thin thicknesses and rich water channels, the membranes exhibit higher permeances than other tight-ultrafiltration membranes and commercial ultrafiltration membranes with similar rejections. Furthermore, thanks to the robust frameworks and good chemical resistance of phenolics, the membranes deliver stable performances in long-term operations, elevated pressures, and acidic conditions. This work provides a facile and universal strategy for the synthesis of membranes with sub-10-nm pores for nanofiltration and tight-ultrafiltration.

1. Introduction

Global water scarcity due to rapid population growth and industrialization appeals for high-efficient water purification technologies [1,2]. Membrane-based separations have been widely used for water treatment benefiting from their unique advantages including high efficiency, low energy consumption, easy maintenance, and continuous operations [3,4]. Precisely recognizing and separating sub-10-nm nanocolloids, biomolecules, and soluble salts from water are of huge significance in wastewater purification and pharmaceutical recovery [5–7]. In general, nanofiltration membranes with pore size smaller than 2 nm have been extensively used in the efficient exclusion of salt ions, but exhibit low fluxes in separation of solutes with larger sizes [8–10]. Alternatively, tight-ultrafiltration membranes with pore size of 2–10 nm are emerging as an indispensable solution for separating nanocolloids and biomolecules according to the size-sieving mechanism [11,12]. Therefore, universal methods for synthesizing nanofiltration and tight-ultrafiltration membranes with sub-10-nm pores can greatly facilitate the tunable separation of different solutes.

Typically, membranes with sub-10-nm pores can be constructed using traditional polymers such as polyethersulfone and polyacrylonitrile through the well-developed phase inversion methods, and ceramics through the sol-gel strategy [13–15]. However, simultaneous optimization of the thickness and the pore size of selective skin layer is difficult, leading to the trade-off effect between flux and rejection. Narrowing the pore size of pre-prepared membranes down to sub-10 nm is another strategy [16–18]. For example, electroless gold deposition was developed to reduce the pore size of block copolymer membranes from 20 nm to 3 nm, contributing to tunable size fractionation of nanoparticles and biomaterials [19]. Nevertheless, thus-prepared membranes suffer from sacrificed porosity, limiting the improvement of fluxes. Recently, advanced two-dimensional (2D) porous nanomaterials have been explored to enable membranes with high porosity and thus high flux. For instance, Jin et al. laminated the tobacco mosaic

* Corresponding author.
** Corresponding author.
E-mail addresses: yongwang@njtech.edu.cn (Y. Wang), txliu@jiangnan.edu.cn (T. Liu).

https://doi.org/10.1016/j.memsci.2021.119858
Received 26 July 2021; Received in revised form 4 September 2021; Accepted 10 September 2021
Available online 13 September 2021

virus mutant nanosheets into membranes with intrinsic pore size of 4 nm for precisely separating nanoparticles, quantum dots, and proteins while exhibiting an ultrahigh permeance of 7000 L/(m^2·h·bar) [20]. Wang et al. controlled the growth of crystalline covalent organic frameworks on porous substrates to fabricate membranes with adjustable pore sizes of 1.8–20 nm ranging from nanofiltration to ultrafiltration and enhanced fluxes [21]. Unfortunately, these methods are challenged by tedious operations and inferior stability of membranes, limiting their real-world applications. Therefore, it is greatly challenging to develop membranes with sub-10-nm pores by simple methods using robust raw materials for high-performance separations.

Thanks to the highly cross-linked frameworks and the good mechanical and chemical stabilities, phenolics have been explored in membrane separations as both selective sieves and substrates [22,23]. The soluble resols as the precursor of phenolics are capable of forming supramolecules with templating polymers by hydrogen-bonding interactions, favoring the processibility of phenolic-based membranes [24,25]. For example, phenolic/polyether supramolecules can self-assemble into cubic mesostructures, and the spin-coated dense membranes can reject multivalent-anion salts derived from the strong charge repulsions between the negatively charged membrane surface and anions [26]. Due to the inertness of phenolic/polymer frameworks, the membranes exhibit good resistance to acid and alkaline solutions with pH 3–9. However, the relatively dense structure leads to an extremely low permeance (<1.5 L/(m^2·h·bar)). Owing to the significant differences in stability between phenolics and templating polymers, various methods such as pyrolysis [27,28], acid extraction [29], and hypercrosslinking [30], have been developed to degrade templating polymers and produce high-porosity phenolics. More importantly, the obtained porous phenolics hold the pore sizes exactly in the range of 2–10 nm, and hence are favorable to deliver tight-ultrafiltration performances [31,32]. Previously, we demonstrated that thus-prepared porous phenolics filled in macroporous membranes can precisely restrain proteins, quantum dots, and poly(ethylene glycol)s (PEGs) [33,34]. Nevertheless, the thicknesses of membranes reach dozens of micrometers, which brings about high mass transfer resistance and limits the improvement in fluxes. Furthermore, we presented a fast solvent evaporation pathway to design an asymmetrically gradient nanoporosity in phenolic membranes with pore size continuously increasing from several nanometers to hundreds of nanometers across the membrane thickness [35,36]. Membranes exhibit unprecedented high fluxes and can efficiently separate species with sizes down to 5 nm. Frustratingly, the interspaces between closely packed phenolic nanoparticles functioning as the nanopores are difficult to be precisely tailored, hindering the application of such membranes in separation of smaller species. To this end, some post-modification methods such as surface coating can endow the membranes with enhanced rejections to dyes for nanofiltration [37], but complicate the fabrication processes. Therefore, simple and universal strategies are highly desired for developing phenolic membranes with tunable sub-10-nm pores for nanofiltration and tight-ultrafiltration while retaining high fluxes.

Herein, we demonstrate a facile and universal method to synthesize nanoporous phenolic membranes with tunable pore sizes and tailored separation performances from nanofiltration to tight-ultrafiltration. The nanoporous phenolic membranes are prepared by spin-coating resol/PEG solution on silica wafers, thermopolymerizing resols to form cross-linked phenolics, and then removing the templating PEGs by acid treatment. The effective pore sizes of membranes can be regulated from 1.3 nm to 9.8 nm by conveniently changing the proportion of PEGs. Membranes thereby exhibit adjustable separation performances to ions, proteins, and nanocolloids with different sizes from nanofiltration to tight-ultrafiltration. Moreover, such membranes show excellent stability against long-term operations, elevated pressures, and strong acids.

2. Experimental section

2.1. Materials

PEGs with molecular weights of 20000 Da (PEG-20000) and 600 Da (PEG-600) were purchased from Sigma-Aldrich Corp. Phenol (99%), aqueous formaldehyde solution (37%), sodium hydroxide (NaOH, 96%), sodium sulphate (Na_2SO_4, 96%), hydrochloric acid (HCl, 36%), sulfuric acid (H_2SO_4, 96%), hydrofluoric acid (HF, 40%), hydrogen peroxide (H_2O_2, 30%), and ethanol (99%) were obtained from Sinopharm Chemical Reagent Co., Ltd. Lysozyme (LZM, M_w = 14300 Da, 98%) and bovine serum albumin (BSA, M_w = 67000 Da, 98%) were supplied by Aladdin. Phosphate buffer solution (PBS) tablets were purchased from MP Biomedicals. The aqueous solutions of monodispersed gold nanoparticles with the particle size of 2 nm and 10 nm (Au-2 nm and Au-10 nm) were obtained from British Biocell International (BBI). Silicon wafers with a top layer of silicon dioxide (~1000 nm in thickness) were provided by HF-Kejing Co., Ltd. Hydrophilic polyvinylidene fluoride (PVDF) macroporous membranes with nominal pore size of 220 nm, porosity of ~70%, and diameter of 2.5 cm were provided by Merck Millipore Ltd. All chemicals were used as received. Home-made deionized water was used in all the experiments.

2.2. Preparation of resol/PEG solution

Resols as the precursor of phenolics were synthesized by polymerizing phenol and formaldehyde in a base-catalyzed reaction [38]. Briefly, 0.61 g of phenol was mixed with 0.13 g of 20 wt% NaOH and 1.05 g of 37 wt% formaldehyde, followed by stirring at 75 °C for 1 h. After cooled down to room temperature, the solution was titrated to pH 7 with 0.6 mol/L HCl and vacuum-dried at 45 °C for 12 h. The products were redissolved in 4.4 mL of ethanol under stirring for 10 min and NaCl precipitates were removed using syringe filters with the pore size of 200 nm, thus producing the resol solutions. Subsequently, PEGs were added to the resol solutions at the PEG/resol mass ratios of 0.5, 1, 2, 3, and 4, respectively. The concentration of the resol/PEG solutions was fixed at 16.2 wt% by adding ethanol. Before use, the resol/PEG solutions were stirred at 40 °C for 10 min to yield homogeneous solutions.

2.3. Preparation of nanoporous phenolic membranes

To fabricate the nanoporous phenolic membranes, 100 μL of the ethanolic resol/PEG solutions were spin-coated on clean silicon wafers at the speed of 2000 r/min for 30 s. Afterwards, the as-coated resol/PEG films were heated at 100 °C for 12 h, and then soaked in 48 wt% H_2SO_4 at 95 °C for 12 h. The nanoporous phenolic membranes supported on silicon wafers were obtained after washing with deionized water and ethanol followed by drying at room temperature for 3 h. To release the nanoporous phenolic membranes from silicon wafers, the membrane-coated silicon wafers were soaked in 5 wt% HF at room temperature for 1 h. It should be noted that HF can cause severe skin burns and eye damage, and is fatal if inhaled or in contact with skin. Wearing protective gloves, clothing, glasses, and mask is required, and the experiment must be carried out in the fume hood. The released nanoporous phenolic membranes were then transferred onto PVDF macroporous substrates and dried at room temperature, producing composite membranes for separation applications.

2.4. Characterizations

Fourier transform infrared spectroscopy (FTIR) spectra were obtained on a ThermoFisher Nicolet 8700 infrared spectrometer at the attenuated total reflection (ATR) mode. X-ray photoemission spectroscopy (XPS) analysis was performed using a Thermo Scientific K-Alpha spectrometer with an Al Kα radiation source ($h\nu$ = 1486.6 eV). The surface charges of the membranes were measured by an Anton Paar

SurPASS electrokinetic analyzer with 1.0 mmol/L KCl solution as electrolyte solution. Scanning electron microscopy (SEM) images were obtained on a Hitachi S-4800 microscope operated at the voltage of 5 kV and the current of 10 μA. The samples were sputter-coated with a thin layer of gold to enhance the conductivity prior to SEM observations. The pore sizes of the nanoporous phenolic membranes were measured using the software *Nano Measurer* based on the corresponding SEM images. The porosities of the nanoporous phenolic membranes were determined using the software *Image Pro Plus*. The thicknesses of the resol/PEG film during heat treatment were characterized using a J. A. Woollam Complete EASE M-2000U spectroscopic ellipsometer with the incidence angle of 65°.

2.5. Separation performances

The water permeances and rejection properties of the membranes were tested using a stirred filtration cell (Amicon 8010, Millipore) under the pressure of 1 bar. The effective membrane area was 4.1 cm^2. Before the water permeance tests, the membranes were prepressed under 1 bar for 30 min to ensure a steady water flow. The water permeance was calculated by equation (1):

$$P = \frac{V}{A \times T \times p} \tag{1}$$

where P (L/(m^2·h·bar)) is the water permeance, V (L) is the volume of water permeated through the membrane, A (m^2) is the effective area of the membrane, T (h) is the operation time, and p (bar) is the transmembrane pressure. Na_2SO_4, Au-2 nm, LZM, BSA, and Au-10 nm were separately used for determining the rejection property of the membranes. To prepare the feed solutions, Na_2SO_4 was dissolved in water at the concentration of 0.1 g/L. A PBS tablet was dissolved in 100 mL of water, and the obtained solution (pH = 7.4) was used to prepare the feed solutions of LZM and BSA at the concentration of 0.5 g/L, respectively. Aqueous solutions of Au-2 nm and Au-10 nm were diluted to the concentration of 0.02 g/L, respectively. Concentrations of LZM, BSA, and Au-10 nm solutions were measured using a UV–vis absorption spectrometer (NanoDrop 2000c, Thermo). Concentrations of Na_2SO_4 and Au-2 nm solutions were calculated from an electrical conductivity meter (S230-K, Mettler-Toledo) and an inductive coupled plasma emission spectrometer (ICAP TQ, Thermo), respectively. The rejection rate was calculated by equation (2):

$$R = \left(1 - \frac{C_{fi}}{C_{fe}}\right) \times 100\% \tag{2}$$

where R (%) is the rejection rate, C_{fi} and C_{fe} are the concentrations of solutes in the filtrate and feed solutions, respectively.

2.6. Performance stabilities

The long-term performance stability of the membranes was evaluated by testing the water permeances and rejection rates to Au-10 nm within 48 h. The pressure resistance test was performed by recording the water fluxes of the membranes under elevated pressures. The chemical stability of the membranes was determined by comparing the water permeances and rejection rates to Au-10 nm of the membranes before and after soaking in 0.1, 0.5, 1.0, and 1.5 mol/L HCl for 120 h, respectively.

3. Results and discussion

3.1. Formation of the nanoporous phenolic membranes

The nanoporous phenolic membrane was fabricated by spin-coating the ethanolic resol/PEG solution on a silicon wafer, followed by thermopolymerization of resols to form phenolics and acid treatment to remove PEGs (Fig. 1). As the precursor of phenolics, the low-molecular-weight and soluble resols possessing abundant hydroxyl groups can interact with the ether groups of PEGs though strong hydrogen bonds [39], forming the resol/PEG supramolecules. The resol/PEG supramolecules with high molecular weight and high viscosity can enable the generation of the uniform resol/PEG film after spinning the resol/PEG solution on a silicon wafer and evaporating the solvent (Fig. 1a–b). Resols were *in-situ* stabilized and confined because of the gelation of PEGs and the strong hydrogen bonds with PEGs, thus leading to the uniformly dispersed resol domains and PEG domains in the resol/PEG film after microphase separation [40]. During the subsequent heating treatment, resols were thermopolymerized by forming methylene groups between benzene rings [41] and turned to insoluble thermosetting phenolics with highly cross-linked frameworks (Fig. 1c). Afterwards, the phenolic/PEG film was subjected to acid treatment to remove templating PEGs by degrading the ether bonds while phenolic matrix was chemically stable and conformal. Consequently, nanopores were generated in the positions previously occupied by PEGs, leading to the nanoporous phenolic membrane (Fig. 1d). Further, the nanoporous phenolic membrane was released from the silicon wafer by HF soaking for dissolving the silicon dioxide layer and transferred onto a macroporous PVDF substrate (Fig. 1e). The obtained composite membrane was used for the evaluation of separation performances.

3.2. PEG removal of the nanoporous phenolic membranes

We firstly used PEG-20000 to prepare the nanoporous phenolic membranes and investigated the changes in chemical compositions of the membranes before and after acid treatment by FTIR spectroscopy to monitor the removal of PEGs. As shown in Fig. 2a, the peaks located at the wavenumbers of 1080 cm^{-1} and 2860 cm^{-1} in the spectrum of the membrane before acid treatment are ascribed to the stretching vibrations of C–O–C and C–H in PEGs, respectively [42,43]. These peaks almost disappear in the spectrum of the membrane after acid treatment, indicating the removal of PEGs. Moreover, phenolics show characteristic peaks located at the wavenumbers of 3360 cm^{-1}, 1645 cm^{-1}, and 1475 cm^{-1} originated from vibrations of –OH, –C═O, and –CH_2-, respectively [44]. These peaks are intact after acid treatment, suggesting that phenolics are acid-resistant and well-preserved. In addition, the peak initially located at the wavenumber of 1610 cm^{-1} corresponding to aromatic C═C of phenolics is shifted to 1595 cm^{-1} after acid treatment [45]. This is because the thermopolymerization of phenolics was continued when membranes were acid-treated at 95 °C, leading to the enhancement of 1,2,4- and 1,2,6-trisubstitution of aromatic rings and highly cross-linked framework structures [24]. Therefore, the FTIR results reveal that PEGs are removed after acid treatment while phenolics are chemically stable, ensuring the fabrication of nanoporous phenolic membranes.

The removal of PEGs after acid treatment was further investigated by XPS analysis. As shown in Fig. 2b, the O 1s peak located at the binding energy of 532.0 eV exhibits significantly weakened intensity in the spectrum of the membrane after acid treatment. Specifically, the atomic ratio of O/C is calculated to be ~0.46 for the membrane before acid treatment, which is decreased to ~0.28 after acid treatment. The decreased proportion of O element indicates the elimination of oxygen-containing groups in the membrane after acid treatment. As shown in Fig. 2c–d, the peak located at the binding energy of 286.3 eV attributed to the C atoms from C–O bonds is greatly reduced after acid treatment, verifying the degradation of C–O–C of PEGs. Therefore, these results confirm the removal of PEGs, which is consistent with the FTIR results. The obtained nanoporous phenolic membrane exhibits negative zeta potentials at pH 3–10, which is indicative of the negatively charged surface property (Fig. S1).

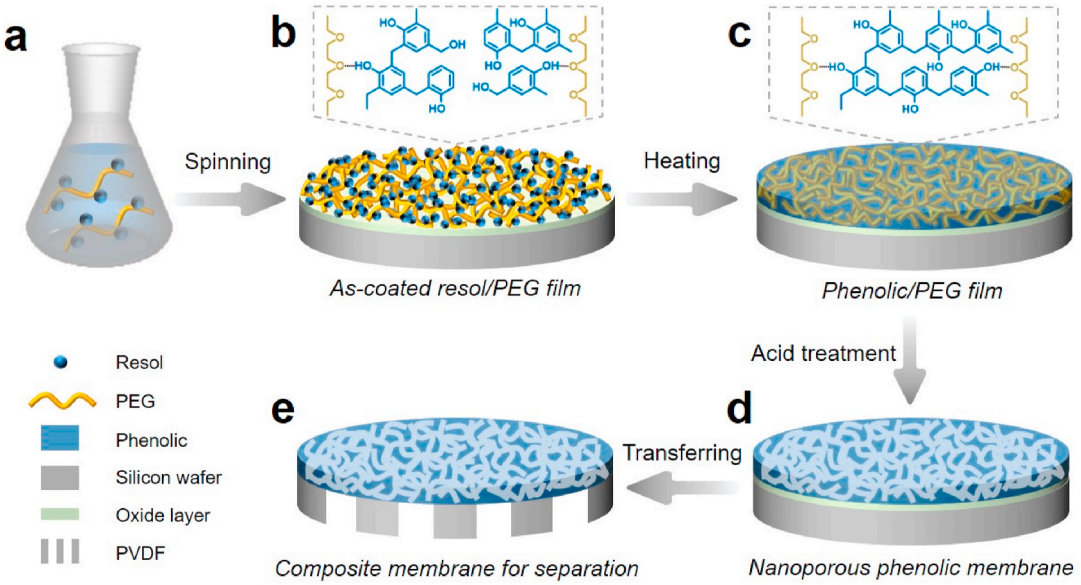

Fig. 1. Schematic illustration for the preparation process of the nanoporous phenolic membranes.

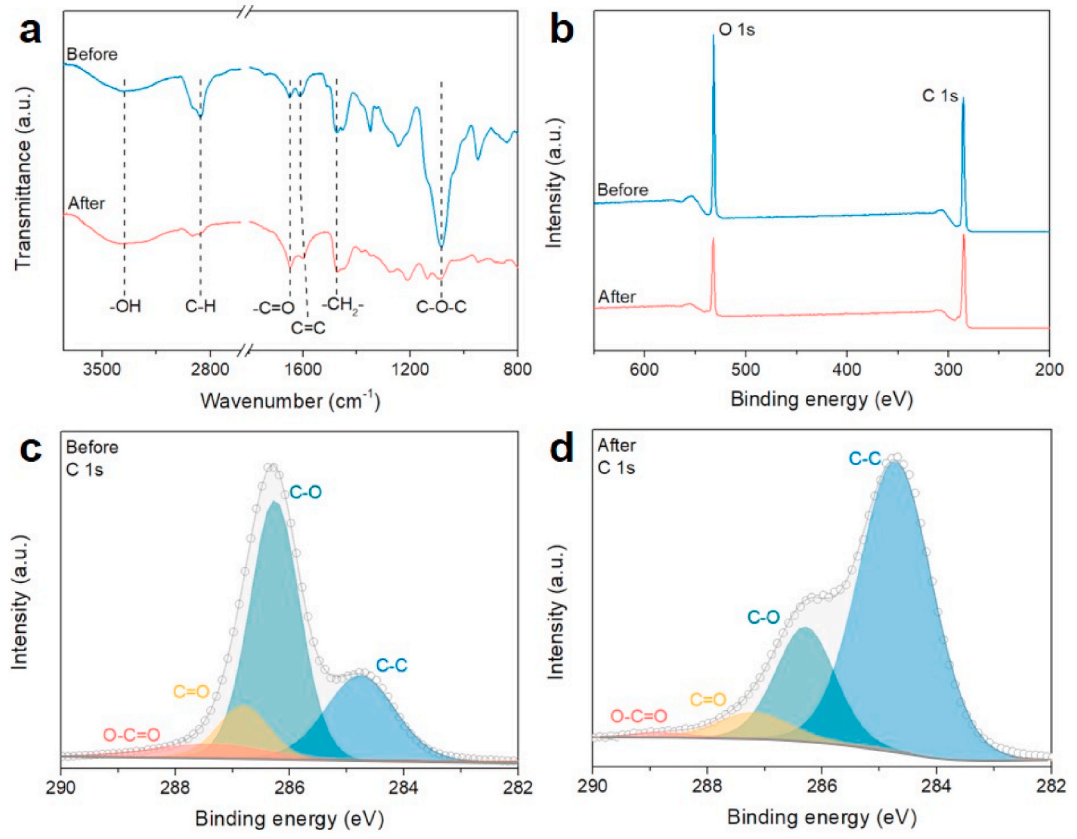

Fig. 2. The compositional changes of the nanoporous phenolic membrane fabricated at the PEG/resol mass ratio of 2 before and after acid treatment. (a) FTIR spectra, (b) XPS survey scan spectra, and high-resolution XPS C1s spectra of the membrane (c) before and (d) after acid treatment.

3.3. Morphologies of the nanoporous phenolic membranes

We firstly examined the morphologies of phenolic/PEG films prepared using PEG-20000 before acid treatment. The as-coated resol/PEG film fabricated at the PEG/resol mass ratio of 2 is in the thickness of ~577 nm (Fig. S2). During the subsequent heating process, the thickness of the resol/PEG film is gradually decreased to ~490 nm due to the thermopolymerization of resols. The obtained phenolic/PEG film after thermopolymerization is dense without pores (Fig. S3).

After acid treatment, PEGs are removed and nanoporous phenolic membranes are generated. We tailored the mass ratios of PEG/resol and prepared a series of nanoporous phenolic membranes. As shown in Fig. 3a–e, when the PEG/resol mass ratio is increased from 0.5 to 4, the obtained membranes exhibit nanopores with enlarged pore sizes. For

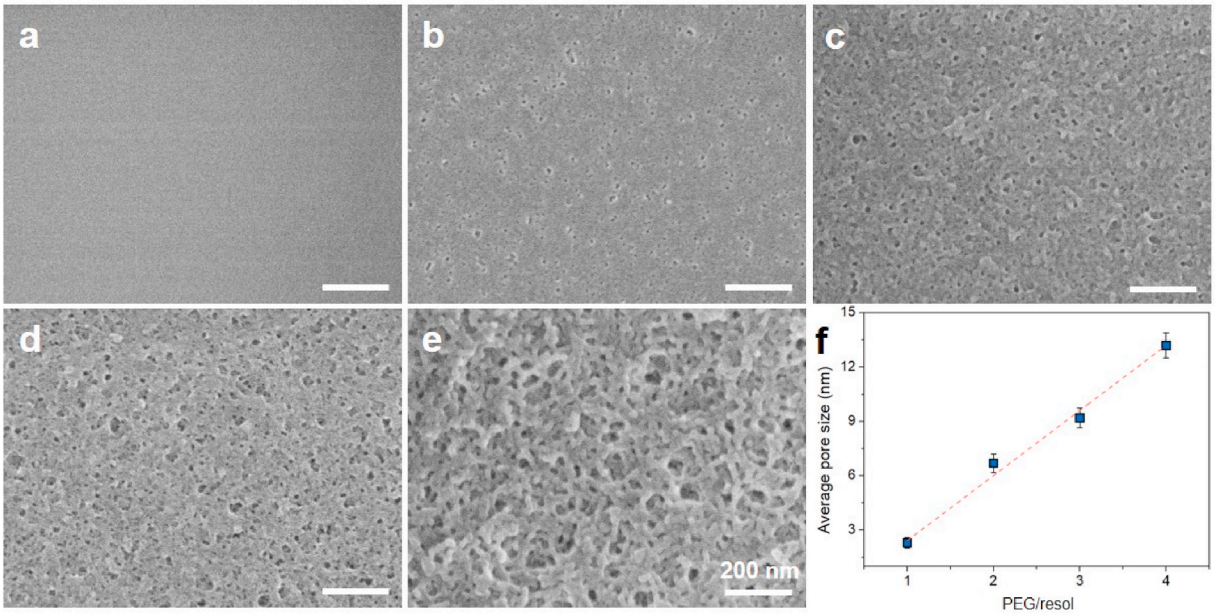

Fig. 3. Morphologies of the nanoporous phenolic membranes. Surface SEM images of the membranes fabricated at the PEG/resol mass ratios of (a) 0.5, (b) 1, (c) 2, (d) 3, and (e) 4. The scale bar in (e) applies to (a–e). (f) Relationship between the average pore size of membranes and the PEG/resol mass ratio.

example, when the PEG/resol mass ratio is 0.5, the obtained membrane shows a relatively dense surface morphology without obvious pore structures. A lot of small round pores can be observed on the surface of the membrane fabricated at the PEG/resol mass ratio of 1. Further, when the PEG/resol mass ratio is increased to 4, the membrane shows a highly pronounced porous structure. The porosities of the membranes fabricated at the PEG/resol mass ratios of 1, 2, 3, and 4 are determined to be 5.4%, 9.4%, 18.0%, and 28.0%, respectively. We further determined the average pore sizes of the membranes and correlated them with the PEG/resol mass ratios. The average pore sizes of the membranes are 2.3 nm, 6.7 nm, 9.2 nm, and 13.2 nm when the PEG/resol mass ratios are 1, 2, 3, and 4, respectively (Fig. S4). As shown in Fig. 2f, the average pore sizes of the membranes are proportional to the PEG/resol mass ratios. With the increase in the PEG/resol mass ratios, the microphase separation of resol/PEG supramolecules leads to larger PEG domains and therefore larger pores after PEG removal. The enlarged pore sizes and well-defined porous structures can also be recognized in the cross-sectional SEM images of the membranes (Fig. S5). Notably, the thicknesses of the membranes are gradually increased with the increase in PEG/resol mass ratios mainly due to the increased viscosities of PEG/resol solutions. However, the influence of thickness on the porous structure is indiscernible since the membranes with varied thicknesses fabricated at the same PEG/resol mass ratio exhibit similar porous structure (Fig. S6). Moreover, if the PEG/resol mass ratio is further increased to 5, we cannot obtain an integrated membrane because PEGs are excessive and continuous phenolic matrix is disturbed into disperse phase (Fig. S7). In addition, when the spin-coating speed is decreased to 300 r/min, the obtained membrane is ununiform in thickness due to the non-Newtonian fluid property of the coated solution before complete gelation (Fig. S8).

Moreover, the molecular weight of PEGs influences the formation of the nanoporous phenolic membranes. When we used PEG-600 at the PEG/resol mass ratio of 2, the obtained membrane exhibits a porous structure with an average pore size of 7.0 nm (Figs. S9a–b), which is similar to that of the membrane prepared using PEG-20000 at the same PEG/resol mass ratio. During the spin-coating process, the solvent evaporates fast and the mobility of PEG chains is rapidly declined [46]. The influence of the molecular weight of PEG on the microphase separation may be inconspicuous in the spin-coated film whereas the proportion of PEG dominates the pore size of the membranes. However, the membrane cannot remain integrated due to the low molecular weight and thus poor film-forming ability (Fig. S9c). In addition, PEGs with molecular weights higher than 20000 Da show decreased solubility in ethanol, leading to poor processibility of their solutions for preparing membranes. Therefore, PEGs play an important role in both porous structures and integrality of the nanoporous phenolic membranes.

3.4. Separation performances of the nanoporous phenolic membranes

To evaluate the separation properties of the nanoporous phenolic membranes, we used HF solution to dissolve the silicon dioxide layer of silicon wafers for detaching the membranes and then transferred the membranes onto macroporous PVDF substrates. As shown in Fig. 4a, the nanoporous phenolic membrane is in the color of light yellow and maintains intact after exfoliating from the silicon wafer. The cross-sectional SEM image in Fig. 4b reveals that the nanoporous phenolic membrane is tightly attached on the PVDF substrate. This is due to the hydrogen-bonding interactions between phenolics and PVDF [34]. The composite structure of thin nanoporous phenolic membrane as the selective layer supported on macroporous substrate is expected to deliver high separation performances.

We firstly measured the water permeances and rejection rates to BSA of the membranes. As shown in Fig. 4c, the water permeances of the membranes are increased with the increasing PEG/resol mass ratios, while the rejection rates are decreased. The membrane fabricated at the PEG/resol mass ratio of 0.5 exhibits a water permeance of 3.7 L/(m^2 h bar), which increased to 163.7 L/(m^2 h bar) for the membrane fabricated at the PEG/resol mass ratio of 1. When the PEG/resol mass ratio is further increased to 2, 3, and 4, the water permeance of the membrane is greatly enhanced to 867.1, 2283.7, and 3344.2 L/(m^2 h bar), respectively. Moreover, the rejection rate of the membrane is gradually declined from 99.8% to 31.1% with the PEG/resol mass ratio increased from 0.5 to 4. The increase in water permeances and the decrease in rejection rates with increasing PEG/resol mass ratios are mainly due to the enlarged pore sizes and rich water channels of the nanoporous phenolic membranes. Larger pore sizes lead to lower mass transfer resistances, resulting in higher water permeances and weaker size-sieving rejection properties.

We then measured the water permeances and rejection rates to BSA of the nanoporous phenolic membranes with varied thicknesses fabricated at the PEG/resol mass ratio of 2. The membranes with thicknesses

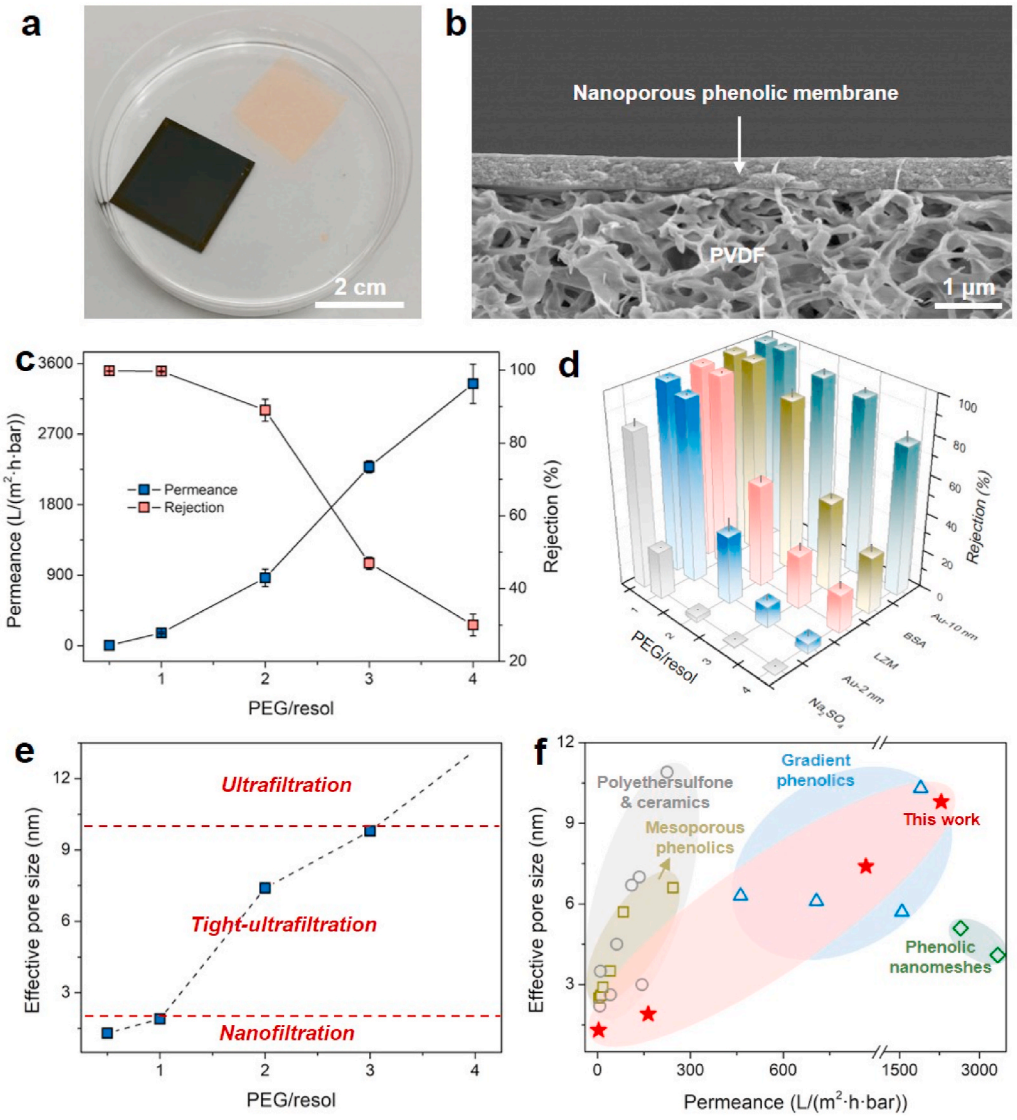

Fig. 4. Separation performances of the nanoporous phenolic membranes. (a) Photograph of the membrane fabricated at the PEG/resol mass ratio of 2 floating on water. (b) Cross-sectional SEM image of the membrane fabricated at the PEG/resol mass ratio of 2 supported on PVDF substrate. (c) Water permeances and rejection rates to BSA, and (d) rejection rates to various solutes of the membranes fabricated at different PEG/resol mass ratios. (e) Effective pore sizes of the membranes fabricated at different PEG/resol mass ratios. (f) Comparison of separation performances between the membranes prepared in this work and other tight-ultrafiltration membranes.

varied from 265 nm to 650 nm can be easily obtained by changing the spin-coating speed in the range of 4000–1000 r/min (Fig. S6). As shown in Fig. S10, the membranes exhibit decreased permeances and increased rejection rates with the increase in thicknesses. For example, the membrane with the thickness of 265 nm shows a high permeance of 1146.7 L/(m^2·h·bar) and a relatively low rejection rate of 70%. When the thickness is increased to 650 nm, the permeance decreases to 701.6 L/(m^2·h bar) due to the higher mass transfer resistances, while the rejection rate increases to 92%. Consequently, tunable separation performances can be realized by manipulating the thicknesses of the membranes.

In addition, we further tested the rejection properties of the membranes to solutes with different sizes ranging from 0.76 nm to 10 nm including Na_2SO_4, Au-2 nm, LZM, and Au-10 nm besides BSA. As shown in Fig. 4d, the membrane fabricated at the PEG/resol mass ratio of 0.5 is capable of rejecting 82.1% of Na_2SO_4 and over 99% of Au-2 nm, LZM, BSA, and Au-10 nm. With the decrease in the PEG/resol mass ratio, the membranes exhibit declined rejection rates to all these solutes. When the PEG/resol mass ratio is decreased to 4, only 0.2% of Na_2SO_4, 4.8% of Au-2 nm, 20.7% of LZM, 31.1% of BSA, and 78.2% of Au-10 nm can be rejected. According to the sizes of solutes and the rejection rates, we determined the effective pore sizes of the membranes which defined as the sizes of solutes with a rejection rate of 90% (Fig. S11). As shown in Fig. 4e, the effective pore sizes of the membranes fabricated at the PEG/resol mass ratios of 0.5, 1, 2, and 3 are 1.3 nm, 1.9 nm, 7.4 nm, and 9.8 nm, respectively. Consequently, tunable effective pore sizes ranging from nanofiltration to tight-ultrafiltration are enabled simply by adjusting the proportion of PEGs. Notably, because of the negative charges of the nanoporous phenolic membranes, the Donnan theory also contributes to the exclusion of negative charged solutes in the nanofiltration range. Moreover, since the membrane fabricated at the PEG/resol mass ratio of 4 shows a rejection rate of 78.2% to Au-10 nm, we conclude that its effective pore size is bigger than 10 nm, which belongs to the ultrafiltration range.

We compared the separation performances of the nanoporous phenolic membranes fabricated in this work with other tight-ultrafiltration membranes in terms of water permeances and effective pore sizes. As shown in Fig. 4f and Table S1, our membranes possessing thin thicknesses and rich water channels exhibit higher water permeances than traditional polyethersulfone and ceramic membranes reported in literature in tight-ultrafiltration range. Moreover, in comparison of mesoporous phenolic membranes with similar water permeances, our membranes display smaller effective pore sizes, which enables high-efficient separations of smaller solutes. In addition, Table S2 shows the comparison of the separation performances between our membranes and some commercial nanofiltration/ultrafiltration

membranes. For example, our membranes can enable 8–20 times higher permeances than commercial ultrafiltration membranes with the molecular-weight-cut-off of 20000 Da. Although the nanofiltration performances of our membranes are inferior to commercial polyamide nanofiltration membranes, it is more important that phenolic membranes for nanofiltration are achieved in this work, broadening the application fields of phenolics. Improved nanofiltration performances are expected to be achieved by further regulating the fabrication parameters.

3.5. Separation performance stabilities

Considering the highly cross-linked frameworks and good chemical resistance of phenolics, we expect that the nanoporous phenolic membranes are highly potential in the real-world applications. To demonstrate this, we firstly evaluated the long-term performance stability of the membranes. As shown in Fig. 5a, the water permeances of the membrane undergo a slight decrease within the initial 1 h due to the pressure-derived compaction. After that, the water permeances maintain unchanged during the testing duration of 48 h. At the same time, the rejection rates of the membrane are steady during the whole test. These results suggest the good performance stability of the membranes. Furthermore, we measured the water fluxes of the membranes under elevated pressures to characterize their pressure resistance. As shown in Fig. 5b, the water fluxes of the membrane are linearly increased under the pressures of 1–5 bar, which is an indicative of the structural robustness of the membranes. Moreover, considering the good acid resistance of phenolics and PVDF, we evaluated the separation performances of the membranes in acid conditions to highlight the potential of the membranes in dealing with acidic industrial effluents. We soaked the membranes in aqueous HCl solutions with different concentrations for 120 h and compared their water permeances and rejection rates to Au-10 nm before and after acid soaking. As shown in Fig. 5c–d, both water permeances and rejection rates are stable before and after soaking in 0.1, 0.5, 1.0, and 1.5 mol/L HCl. In addition, the pore structures of the membranes are unchanged after acid soaking (Fig. S12). These results manifest the good chemical stability of the membranes in acid conditions. Therefore, we conclude that the nanoporous phenolic membranes are structural stable against long-term operations, elevated pressures, and strong acids, facilitating the application of the membranes in practical processes. Prospectively, large-scale production of the nanoporous phenolic membranes can be enabled by altering the unfavorable HF-etching process, for example, using water-soluble substrates for transferring the membranes or directly preparing the membranes on porous substrates.

4. Conclusion

In conclusion, we report on the preparation of nanoporous phenolic membranes with tunable pore sizes by using resols as the precursor and PEGs as the templating polymer. The hydrogen-bonded resol/PEG can form thin films after spin-coating, and transform to phenolic/PEG film after heating to thermopolymerize resols. The templating PEGs are then removed by acid treatment, leading to the nanopores in phenolic matrixes. The prepared nanoporous phenolic membranes show adjustable pore sizes by simply changing the mass ratio of PEG/resol. Accordingly, membranes exhibit tunable separation performances with high water permeances and effective pore sizes of 1.3–9.8 nm ranging from nanofiltration to tight-ultrafiltration. Thanks to the robust frameworks and good chemical stability of phenolics, membranes are resistant against long-term operations, elevated pressures, and strong acids. This work suggests an easy method to fabricate high-performance phenolic membranes for nanofiltration and tight-ultrafiltration, and reveals the possibility of such membranes in real-world applications.

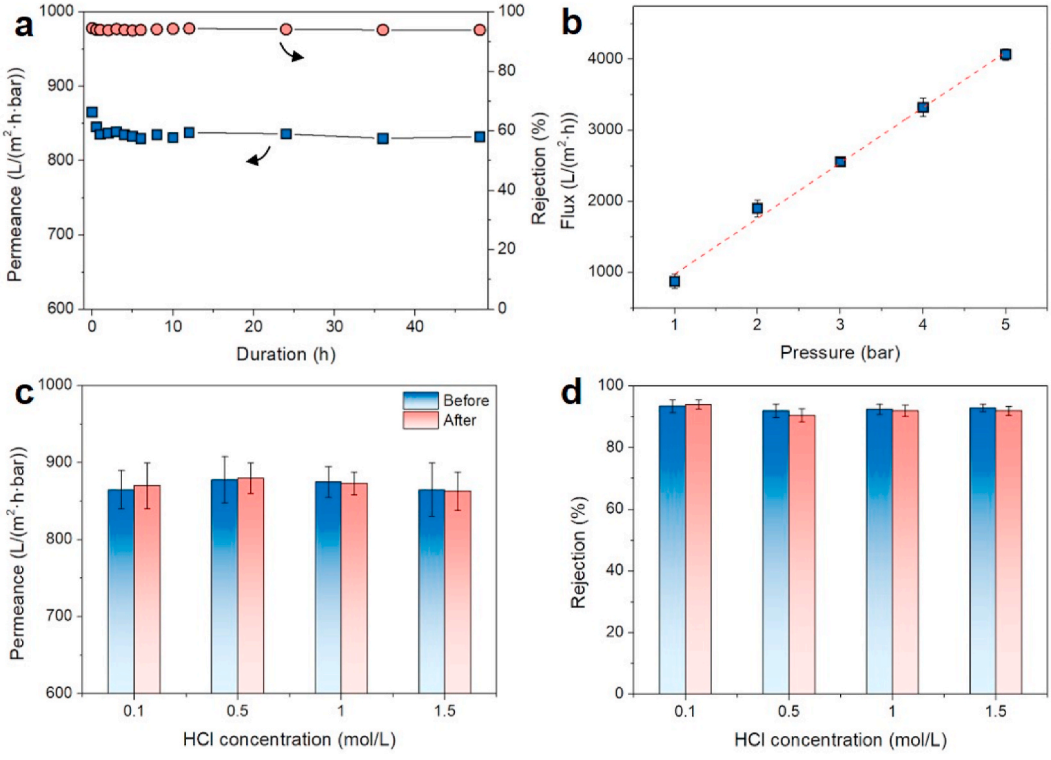

Fig. 5. Separation performance stabilities of the nanoporous phenolic membrane fabricated at the PEG/resol mass ratio of 2. (a) Water permeances and rejection rates to Au-10 nm of the membrane in long-term operation. (b) Water fluxes of the membrane under elevated pressures. (c) Water permeances and (d) rejection rates to Au-10 nm of the membrane before (blue) and after (red) soaking in HCl solutions with different concentrations for 120 h, respectively. (For interpretation of the references to color in this figure legend, the reader is referred to the Web version of this article.)

Author statement

Qianqian Lan: Conceptualization, Methodology, Software, Investigation, Writing - Original Draft, Project administration, Funding acquisition, Chao Feng: Software, Formal analysis, Kaiqin Ou: Validation, Investigation, Zicheng Wang: Investigation, Yong Wang: Resources, Writing - Review & Editing, Supervision, Funding acquisition, Tianxi Liu: Resources, Writing - Review & Editing, Supervision.

Declaration of competing interest

The authors declare that they have no known competing financial interests or personal relationships that could have appeared to influence the work reported in this paper.

Acknowledgment

Financial supports from the National Natural Science Foundation of China (22008086, 21825803), the China Postdoctoral Science Foundation (2020M671332), and the Jiangsu Postdoctoral Science Foundation (2020Z210) are gratefully acknowledged.

Appendix A. Supplementary data

Supplementary data to this article can be found online at https://doi.org/10.1016/j.memsci.2021.119858.

References

[1] M. Elimelech, W.A. Phillip, The future of seawater desalination: energy, technology, and the environment, Science 333 (2011) 712–717.
[2] Z. Xia, Y. Zhao, S.B. Darling, Covalent organic frameworks for water treatment, Adv. Mater. Interfaces 8 (2020) 2001507.
[3] A. Lee, J.W. Elam, S.B. Darling, Membrane materials for water purification: design, development, and application, Environ. Sci.: Water Res. Technol. 2 (2016) 17–42.
[4] Y. Lv, J. Xia, Y. Yang, Y. Chen, T. Liu, Thin-film composite membranes with mineralized nanofiber supports for highly efficient nanofiltration, Compos. Commun. 24 (2021) 100695.
[5] Z. Tan, S. Chen, X. Peng, L. Zhang, C. Gao, Polyamide membranes with nanoscale Turing structures for water purification, Science 360 (2018) 518–521.
[6] L. Ding, Y. Wei, Y. Wang, H. Chen, J. Caro, H. Wang, A two-dimensional lamellar membrane: mxene nanosheet stacks, Angew. Chem. Int. Ed. 56 (2017) 1825–1829.
[7] Q. Lan, Y. Wang, Carbonization of gradient phenolics filled in macroporous substrates for high-flux tight membranes: toward ultrafiltration of polypeptides, J. Membr. Sci. 590 (2019) 117309.
[8] Z.Y. Ma, X. Zhang, C. Liu, S.N. Dong, J. Yang, G.P. Wu, Z.K. Xu, Polyamide nanofilms synthesized via controlled interfacial polymerization on a "jelly" surface, Chem. Commun. 56 (2020) 7249–7252.
[9] S. Karan, Z. Jiang, A.G. Livingston, Sub-10 nm polyamide nanofilms with ultrafast solvent transport for molecular separation, Science 348 (2015) 1347–1351.
[10] H. Zhang, Q. He, J. Luo, Y. Wan, S.B. Darling, Sharpening nanofiltration: strategies for enhanced membrane selectivity, ACS Appl. Mater. Interfaces 12 (2020) 39948–39966.
[11] J. Winter, B. Barbeau, P. Berube, Nanofiltration and tight ultrafiltration membranes for natural organic matter removal-contribution of fouling and concentration polarization to filtration resistance, Membranes 7 (2017) 34.
[12] S. Wu, Z. Wang, S. Xiong, Y. Wang, Tailoring TiO_2 membranes for nanofiltration and tight ultrafiltration by leveraging molecular layer deposition and crystallization, J. Membr. Sci. 578 (2019) 149–155.
[13] G. Jiang, S. Zhang, Y. Zhu, S. Gao, H. Jin, L. Luo, F. Zhang, J. Jin, Hydrogel-embedded tight ultrafiltration membrane with superior anti-dye-fouling property for low-pressure driven molecule separation, J. Mater. Chem. 6 (2018) 2927–2934.
[14] J. Lin, W. Ye, M.-C. Baltaru, Y.P. Tang, N.J. Bernstein, P. Gao, S. Balta, M. Vlad, A. Volodin, A. Sotto, P. Luis, A.L. Zydney, B. Van der Bruggen, Tight ultrafiltration membranes for enhanced separation of dyes and Na_2SO_4 during textile wastewater treatment, J. Membr. Sci. 514 (2016) 217–228.
[15] H. Qin, W. Guo, P. Gao, H. Xiao, Customization of ZrO_2 loose/tight bilayer ultrafiltration membranes by reverse micelles-mediated aqueous sol-gel process for wastewater treatment, J. Eur. Ceram. Soc. 41 (2021) 2724–2733.
[16] A. Mautner, K.Y. Lee, T. Tammelin, A.P. Mathew, A.J. Nedoma, K. Li, A. Bismarck, Cellulose nanopapers as tight aqueous ultra-filtration membranes, React. Funct. Polym. 86 (2015) 209–214.
[17] H. Yu, X. Qiu, N. Moreno, Z. Ma, V.M. Calo, S.P. Nunes, K.V. Peinemann, Self-assembled asymmetric block copolymer membranes: bridging the gap from ultra- to nanofiltration, Angew. Chem. Int. Ed. 54 (2015) 13937–13941.
[18] Y. Gu, U. Wiesner, Tailoring pore size of graded mesoporous block copolymer membranes: moving from ultrafiltration toward nanofiltration, Macromolecules 48 (2015) 6153–6159.
[19] H. Yu, X. Qiu, S.P. Nunes, K.V. Peinemann, Self-assembled isoporous block copolymer membranes with tuned pore sizes, Angew. Chem. Int. Ed. 53 (2014) 10072–10076.
[20] S. Zhang, J. Zhang, W. Fang, Y. Zhang, Q. Wang, J. Jin, Ultralarge single-layer porous protein nanosheet for precise nanosize separation, Nano Lett. 18 (2018) 6563–6569.
[21] X. Shi, A. Xiao, C. Zhang, Y. Wang, Growing covalent organic frameworks on porous substrates for molecule-sieving membranes with pores tunable from ultra- to nanofiltration, J. Membr. Sci. 576 (2019) 116–122.
[22] Q. Lan, Z. Zhang, F. Xu, M. Wei, Y. Wang, Nanomeshes with sub-10 nm pores by glycerol-triggered 2D assembly in liquid phases for fast and selective membranes, Nano Lett. 21 (2021) 3302–3309.
[23] Y. Yang, Q. Lan, Y. Wang, Gradient nanoporous phenolics as substrates for high-flux nanofiltration membranes by layer-by-layer assembly of polyelectrolytes, Chin. J. Chem. Eng. 28 (2020) 114–121.
[24] X. Huo, Q. Lan, Y. Wang, In situ cavitation of phenolic supramolecules with PEO-PPO-PEO block copolymers by Friedel-Crafts alkylation toward ordered nanoporous polymers, Ind. Eng. Chem. Res. 55 (2016) 6398–6404.
[25] Y. Wan, Y. Shi, D. Zhao, Supramolecular aggregates as templates: ordered mesoporous polymers and carbons, Chem. Mater. 20 (2008) 932–945.
[26] Q. Li, G. Chen, L. Liu, X. Wang, Fabrication of phenolic resin based desalting membrane with ordered mesostructure and excellent chlorine resistance, J. Membr. Sci. 550 (2017) 502–509.
[27] Q. Zhang, F. Matsuoka, H.S. Suh, P.A. Beaucage, S. Xiong, D.M. Smilgies, K.W. Tan, J.G. Werner, P.F. Nealey, U.B. Wiesner, Pathways to mesoporous resin/carbon thin films with alternating gyroid morphology, ACS Nano 12 (2018) 347–358.
[28] L. Liu, X. Yang, Y. Xie, H. Liu, X. Zhou, X. Xiao, Y. Ren, Z. Ma, X. Cheng, Y. Deng, D. Zhao, A universal lab-on-salt-particle approach to 2D single-layer ordered mesoporous materials, Adv. Mater. 32 (2020) 1906653.
[29] X. Zhuang, X. Qian, J. Lv, Y. Wan, An alternative method to remove PEO-PPO-PEO template in organic-inorganic mesoporous nanocomposites by sulfuric acid extraction, Appl. Surf. Sci. 256 (2010) 5343–5348.
[30] J. Zhang, Z.A. Qiao, S.M. Mahurin, X. Jiang, S.H. Chai, H. Lu, K. Nelson, S. Dai, Hypercrosslinked phenolic polymers with well-developed mesoporous frameworks, Angew. Chem. Int. Ed. 54 (2015) 4582–4586.
[31] Y. Liang, R. Fu, D. Wu, Reactive template-induced self-assembly to ordered mesoporous polymeric and carbonaceous materials, ACS Nano 7 (2013) 1748–1754.
[32] Y. Fang, Y. Lv, J. Tang, H. Wu, D. Jia, D. Feng, B. Kong, Y. Wang, A.A. Elzatahry, D. Al-Dahyan, Q. Zhang, G. Zheng, D. Zhao, Growth of single-layered two-dimensional mesoporous polymer/carbon films by self-assembly of monomicelles at the interfaces of various substrates, Angew. Chem. Int. Ed. 54 (2015) 8425–8429.
[33] Q. Lan, N. Yan, Y. Wang, Tight ultrafiltration membranes of mesoporous phenolic resin filled in macroporous substrates, J. Membr. Sci. 533 (2017) 96–102.
[34] Q. Lan, Z. Wang, Y. Wang, Mesoporous phenolics filled in macroporous membranes for tunable tight-ultrafiltration, Chem. Eng. Sci. 187 (2018) 98–106.
[35] L. Guo, Y. Yang, F. Xu, Q. Lan, M. Wei, Y. Wang, Design of gradient nanopores in phenolics for ultrafast water permeation, Chem. Sci. 10 (2019) 2093–2100.
[36] Q. Lan, Y. Yang, L. Guo, Y. Wang, Gradient nanoporous phenolics filled in macroporous substrates for highly permeable ultrafiltration, J. Membr. Sci. 576 (2019) 123–130.
[37] L. Guo, Y. Yang, Y. Wang, Single-step coating of polyethylenimine on gradient nanoporous phenolics for tight membranes with ultrahigh permeance, J. Membr. Sci. 587 (2019) 117172.
[38] D. Feng, Y. Lv, Z. Wu, Y. Dou, L. Han, Z. Sun, Y. Xia, G. Zheng, D. Zhao, Free-standing mesoporous carbon thin films with highly ordered pore architectures for nanodevices, J. Am. Chem. Soc. 133 (2011) 15148–15156.
[39] J. Liu, T. Yang, D.-W. Wang, G.Q. Lu, D. Zhao, S.Z. Qiao, A facile soft-template synthesis of mesoporous polymeric and carbonaceous nanospheres, Nat. Commun. 4 (2013) 2798.
[40] Y. Wang, Nondestructive creation of ordered nanopores by selective swelling of block copolymers: toward homoporous membranes, Acc. Chem. Res. 49 (2016) 1401–1408.
[41] Y. Meng, D. Gu, F. Zhang, Y. Shi, H. Yang, Z. Li, C. Yu, B. Tu, D. Zhao, Ordered mesoporous polymers and homologous carbon frameworks: amphiphilic surfactant templating and direct transformation, Angew. Chem. Int. Ed. 44 (2005) 7053–7059.

[42] H. Zuo, X. Chen, Y. Ding, L. Cui, B. Fan, L. Pan, K. Zhang, Novel designed PEG-dicationic imidazolium-based ionic liquids as effective plasticizers for sustainable polylactide, Chin. J. Chem. 39 (2021) 2234–2240.
[43] Y. Wu, M. Fei, T. Chen, R. Qiu, W. Liu, Biocomposites from bamboo fibers and palm oil-based thermosets: effects of natural phenolic cross-linkers, Compos. Commun. 22 (2020) 100489.
[44] Z.L. Yu, G.C. Li, N. Fechler, N. Yang, Z.Y. Ma, X. Wang, M. Antonietti, S.H. Yu, Polymerization under hypersaline conditions: a robust route to phenolic polymer-derived carbon aerogels, Angew. Chem. Int. Ed. 55 (2016) 14623–14627.
[45] Y. Meng, D. Gu, F. Zhang, Y. Shi, L. Cheng, D. Feng, Z. Wu, Z. Chen, Y. Wan, A. Stein, D. Zhao, A family of highly ordered mesoporous polymer resin and carbon structures from organic-organic self-assembly, Chem. Mater. 18 (2006) 4447–4464.
[46] J. Yin, X. Yao, J.-Y. Liou, W. Sun, Y.-S. Sun, Y. Wang, Membranes with highly ordered straight nanopores by selective swelling of fast perpendicularly aligned block copolymers, ACS Nano 7 (2013) 9961–9974.